INTERNATIONAL JOURNAL FOR NUMERICAL METHODS IN FLUIDS, VOL. 3, 33–60 (1983)

FORMULATION OF A LINEAR THREE-DIMENSIONAL HYDRODYNAMIC SEA MODEL USING A GALERKIN-EIGENFUNCTION METHOD

A. M. DAVIES

Institute of Oceanographic Sciences, Bidston Observatory, Birkenhead, Merseyside L43 7RA, England

SUMMARY

The three dimensional linear hydrodynamic equations which describe wind induced flow in a sea are solved using the Galerkin method. A basis set of eigenfunctions is used in the calculation. These eigenfunctions are determined numerically using an expansion of B-splines.

Using the Galerkin method the problem of wind induced flow in a rectangular basin is examined in detail. A no-slip bottom boundary condition with a vertically varying eddy viscosity distribution is employed in the calculation. With a low (of order 1 cm^2/s) value of viscosity at the sea bed there is high current shear in this region. Viscosities of the order of 1 cm^2/s near the sea bed together with high current shear in this region are physically realistic and have been observed in the sea.

In order to accurately compute the eigenfunctions associated with large (of order 2000 cm^2/s at the sea surface to 1 cm^2/s at the sea bed) vertical variation of viscosity, an expansion of the order of thirty-five B-splines has to be used. The spline functions are distributed through the vertical so as to give the maximum resolution in the high shear region near the sea bed.

Calculations show that in the case of a no-slip bottom boundary condition, with an associated region of high current shear near the sea bed, the Galerkin method with a basis set of the order of ten eigenfunctions (a Galerkin–eigenfunction method) yields an accurate solution of the hydrodynamic equations. However, solving the same problem using the Galerkin method with a basis set of B-splines, requires an expansion of the order of thirty-five spline functions in order to obtain the same accuracy.

Comparisions of current profiles and time series of sea surface elevation computed using a model with a slip bottom boundary condition and a model with a no-slip boundary condition have been made. These comparisions show that consistent solutions are obtained from the two models when a physically relistic coefficient of bottom friction is used in the slip model, and a physically realistic bottom roughness length and thickness of the bottom boundary layer are employed in the no-slip model.

KEY WORDS Vertical Eddy Viscosity Galerkin Method Hydrodynamic Model Eigenfunction Currents Roughness length

1. INTRODUCTION

The numerical solution of the three dimensional hydrodynamic equations which describe the motion of the sea, using either grid boxes or multiple layers in the vertical is now well established. With these methods the current is only evaluated at discrete points through the vertical in a grid box model, or a mean over each layer in a layered model. For problems in which a boundary layer of high current shear occurs, such as the region near the sea bed, it is necessary to increase the resolution in this area.

Improved resolution within the boundary layer can be obtained by using a transformation, (such as a logarithmic compression near the sea bed[1]) to increase accuracy in this region, although at the expense of reduced resolution elsewhere. Alternatively, improved resolution can be obtained by using a very fine grid spacing at the sea bed. However, increasing the grid resolution by this means involves a larger number of point values in the vertical, which have

0271–2091/83/010033–28$02.80

Received 26 August 1981
Revised 23 March 1982

to be integrated through time as the solution evolves. Naturally, as the grid resolution is refined, the associated computer time required to integrate the equations increases rapidly.

An alternative to using grid boxes or layers in the vertical is to expand the horizontal components of current in terms of time and horizontally varying coefficients and functions through the vertical (the basis functions). The coefficients in the expansion can then be obtained using the Galerkin method.[2–4] By this means a continuous current profile from sea surface to sea bed can be computed.

In theory the choice of basis functions is arbitrary, however in practice their functional form is important,[4] particularly in the high shear layer at the sea bed, which occurs when currents are computed using a no-slip bottom boundary condition.

In this paper the Galerkin method is used to solve the three dimensional hydrodynamic equations which describe wind induced flow in a rectangular basin. Unlike previous application of the Galerkin method to this problem,[2–4] the basis functions are not chosen in an arbitrary manner, but are the eigenfunctions of an eigenvalue problem involving the vertical eddy viscosity. By this means in a linear model a set of uncoupled partial differential equations is obtained. (The use of the Galerkin method with an arbitrary basis set yields a set of coupled equations).

The choice of a basis set of eigenfunctions, is not new; it is the essential feature of the eigenfunction method used by Heaps.[5,6] The eigenfunctions used by Heaps however were determined analytically, and consequently the vertical variation of viscosity was restricted to a profile for which an analytical solution could be obtained. In the method developed in this paper the eigenfunctions are determined numerically, therefore the complex vertical variations of viscosity which are found in nature[7,8] can be included in the model.

The eigenfunctions used in this paper are calculated in terms of an expansion of B-splines. These functions are piecewise polynomials which are only non-zero over a small interval of space. This piecewise property can be used to advantage in the numerical calculation of the eigenfunctions, since it enables the number of B-splines in regions where a high vertical resolution is required to be increased.

Since the solution of the eigenvalue problem requires very little computer time, the calculation can be repeated using various vertical distributions of B-splines. By this means it is possible to check that the expansion of B-splines has converged and that the eigenfunctions have been accurately determined.

The eigenfunction method developed in this paper is used to compute wind induced currents within a closed rectangular flat bottomed basin. The dimensions of the basin approximate those of the North Sea.

Calculations show that current profiles converge rapidly as the number of eigenfunctions in the basis set increases.

Current profiles and time variations of sea surface elevation, computed using no-slip and slip bottom boundary conditions are compared in Section 4 of this paper. These comparisions show that provided physically realistic values of bottom friction (in the slip model) and thickness of the bottom boundary layer and roughness length (in the no-slip model) are used, then the two types of model are physically consistent.

2. FORMULATION OF THE HYDRODYNAMIC EQUATIONS

(a) *Basic equations*

The equations of continuity and motion for a homogeneous sea, neglecting non-linear terms, and the direct influence of the tide-generating forces, and using for consistency the

same Cartesian Co-ordinate system as that employed by Heaps[5,6] and Davies[3,9] may be written as:

$$\frac{\partial}{\partial x}\int_0^h u\,dz+\frac{\partial}{\partial y}\int_0^h v\,dz+\frac{\partial \zeta}{\partial t}=0 \tag{1}$$

$$\frac{\partial u}{\partial t}-\gamma v=-g\frac{\partial \zeta}{\partial x}+\frac{\partial}{\partial z}\left(N\frac{\partial u}{\partial z}\right) \tag{2}$$

$$\frac{\partial v}{\partial t}+\gamma u=-g\frac{\partial \zeta}{\partial y}+\frac{\partial}{\partial z}\left(N\frac{\partial v}{\partial z}\right) \tag{3}$$

where in these equations:

t	denotes time
x, y, z	a left handed set of Cartesian co-ordinates, with z the depth below the undisturbed surface and x, y co-ordinates in the horizontal plane
h	the undisturbed depth of water
ζ	elevation above the undisturbed depth
u, v, the x and y	components of current at depth z
γ	geostrophic coefficient
g	acceleration due to gravity
N	coefficient of vertical eddy viscosity

In these equations γ and g are constants. The variables u, v and N vary with x, y, z and t. Depth h is a function in general of x and y; and ζ varies with x, y and t.

In order to solve equations (1)–(3) for ζ, u, v, boundary conditions have to be specified at the sea surface and at the sea bed.

The surface conditions, evaluated at $z=0$, are:

$$-\rho\left(N\frac{\partial u}{\partial z}\right)_0=F_s, \qquad -\rho\left(N\frac{\partial v}{\partial z}\right)_0=G_s \tag{4}$$

where F_s, G_s denote the components of wind stress acting on the water surface in the x and y directions; ρ, the density of sea water, is assumed constant. Suffix 0 denotes evaluation at $z=0$.

Similarly at the sea bed

$$-\rho\left(N\frac{\partial u}{\partial z}\right)_h=F_B, \qquad -\rho\left(N\frac{\partial v}{\partial z}\right)_h=G_B \tag{5}$$

where F_B, G_B denote the components of bottom friction in the x and y directions.

Assuming a linear slip condition at the sea bed:

$$F_B=k\rho u_h, \qquad G_B=k\rho v_h \tag{6}$$

with k the coefficient of linear bottom friction.

A quadratic law at the sea bed may be applied rather than the linear law. In this case

$$F_B=K\rho u_h(u_h^2+v_h^2)^{1/2}, \qquad G_B=K\rho v_h(u_h^2+v_h^2)^{1/2} \tag{7}$$

with K the coefficient of non-linear bottom friction.

An alternative bottom boundary condition, to those given by (6) and (7) is a no-slip condition, namely:

$$u_h=v_h=0 \tag{8}$$

(b) *Application of Galerkin method, with an arbitrary set of basis functions*

We now consider the solution of equations (1)–(3) using the Galerkin method.

Expanding the two components of velocity in terms of m depth-dependent functions $f_r(s)$ (the basis functions) and coefficients $A_r(x, y, t)$ and $B_r(x, y, t)$ varying with horizontal position and through time, gives

$$u(x, y, z, t) = \sum_{r=1}^{m} A_r(x, y, t) f_r(s) \tag{9}$$

$$v(x, y, z, t) = \sum_{r=1}^{m} B_r(x, y, t) f_r(s) \tag{10}$$

where

$$s = z/h \tag{11}$$

This relation transforms the interval $0 \leqslant z \leqslant h$ (which varies in general with horizontal position x, y due to variations in the sea bed depth h) into the constant interval $0 \leqslant s \leqslant 1$.

Substituting (9) and (10) into equation (1), transformation using (11), gives

$$\frac{\partial \zeta}{\partial t} + \sum_{r=1}^{m} \left[\frac{\partial}{\partial x} \left\{ A_r h \int_0^1 f_r \, ds \right\} + \frac{\partial}{\partial y} \left\{ B_i h \int_0^1 f_r \, ds \right\} \right] = 0 \tag{12}$$

Considering the u-equation of motion (equation (2)). Applying the Galerkin method, we multiply equation (2) by f_k, transform from the region z to the region s, using equation (11) and integrate with respect to s over the region 0 to 1. (For details see References 3–4.) Dividing the resulting equation through by h, gives,

$$\int_0^1 \frac{\partial u}{\partial t} f_k \, ds = \gamma \int_0^1 v f_k \, ds - g \frac{\partial \zeta}{\partial x} \int_0^1 f_k \, ds + \frac{1}{h^2} \int_0^1 \frac{\partial}{\partial s} \left(N \frac{\partial u}{\partial s} \right) f_k \, ds, \qquad k = 1, 2, \ldots, m \tag{13}$$

Integrating the last term in (13) by parts, gives

$$\int_0^1 \frac{\partial u}{\partial t} f_k \, ds = \gamma \int_0^1 v f_k \, ds - g \frac{\partial \zeta}{\partial x} \int_0^1 f_k \, ds + \frac{N}{h^2} \frac{\partial u}{\partial s} f_k \Big|_1 - \frac{N}{h^2} \frac{\partial u}{\partial s} f_k \Big|_0 - \frac{1}{h^2} \int_0^1 N \frac{\partial u}{\partial s} \frac{df_k}{ds} \, ds, \qquad k = 1, 2, \ldots, m \tag{14}$$

Eliminating the terms $N \frac{\partial u}{\partial s}\Big|_1$ and $N \frac{\partial u}{\partial s}\Big|_0$ in (14) using transformation (11) and boundary condition (4) and (5) gives

$$\int_0^1 \frac{\partial u}{\partial t} f_k \, ds = \gamma \int_0^1 v f_k \, ds - g \frac{\partial \zeta}{\partial x} \int_0^1 f_k \, ds - \frac{F_B}{\rho h} f_k(1) + \frac{F_s}{\rho h} f_k(0) - \frac{1}{h^2} \int_0^1 N \frac{\partial u}{\partial s} \frac{df_k}{ds} \, ds, \qquad k = 1, 2, \ldots, m \tag{15}$$

Substituting expansions (9) and (10) into (15), gives

$$\sum_{r=1}^{m} \frac{\partial A_r}{\partial t} \int_0^1 f_r f_k \, ds = \gamma \sum_{r=1}^{m} B_r \int_0^1 f_r f_k \, ds - g \frac{\partial \zeta}{\partial x} \int_0^1 f_k \, ds - \frac{F_B}{\rho h} f_k(1) + \frac{F_s}{\rho h} f_k(0) - \frac{1}{h^2} \sum_{r=1}^{m} A_r \int_0^1 N \frac{df_r}{ds} \frac{df_k}{ds} \, ds \qquad k = 1, 2, \ldots, m \tag{16}$$

In order to use equation (16) to advance the coefficients A_r through time, it is necessary to compute the integrals involving N. For the general case in which N varies with x, y, z and t, the problem of recomputing these integrals through time and space, can be avoided by expanding the viscosity in terms of coefficients $E_j(x, y, t)$ and vertically varying functions $\Phi_j(s)$,[2,3] thus

$$N(x, y, s, t) = \sum_{j=1}^{m'} E_j(x, y, t)\Phi_j(s) \tag{17}$$

where m' is not necessarily equal to m.

The formulation and solution of the equations of motion using the Galerkin method with eddy viscosity given by (17) has been given in detail for the non-linear equations by Davies[3] and for the linear equations by Davies and Owen[4] and Davies.[2]

Although equation (17) allows for a completely general form of eddy viscosity; in practical computations the vertical variation of N is usually fixed although its magnitude varies with horizontal position and time, see for example References 10 and 11. For the case in which the vertical variation of N is fixed, we have,

$$N(x, y, s, t) = \alpha(x, y, t)\phi(s) \tag{18}$$

where ϕ is a fixed function, representing the vertical variation of N.

Substituting equation (18) into (16), gives

$$\sum_{r=1}^{m} \frac{\partial A_r}{\partial t} \int_0^1 f_r f_k \, ds = \gamma \sum_{r=1}^{m} B_r \int_0^1 f_r f_k \, ds - g\frac{\partial \zeta}{\partial x} \int_0^1 f_k \, ds$$
$$- \frac{F_B}{\rho h} f_k(1) + \frac{F_s}{\rho h} f_k(0) - \frac{\alpha}{h^2} \sum_{r=1}^{m} A_r \int_0^1 \phi \frac{df_r}{ds} \frac{df_k}{ds} ds, \qquad k = 1, 2, \ldots, m \tag{19}$$

In general the basis functions f_r can be chosen in an arbitrary manner. Davies[9] used a basis set of piecewise functions (B-splines), whereas Davies and Owen[4] used continuous functions.

(c) *Application of the Galerkin method with a basis set of eigenfunctions*

(i) *Formulation and solution of the eigenvalue problem.* With arbitrary basis functions the m simultaneous equations given by (19) are coupled together. However for the case in which the vertical variation of N does not vary with horizontal position or time, (equation (18)) it is possible to uncouple these equations by choosing the basis functions f_r to be eigenfunctions, with corresponding eigenvalues $\tilde{\varepsilon}_r$ of an eigenvalue problem involving the vertical eddy viscosity, of the form

$$\frac{d}{ds}\left[N\frac{df}{ds}\right] = -\tilde{\varepsilon} f \tag{20}$$

Substituting (18) into (20) gives

$$\alpha(x, y, t)\frac{d}{ds}\left[\phi\frac{df}{ds}\right] = -\tilde{\varepsilon} f \tag{21}$$

Since α is a function of x, y, t it only affects the magnitude of the eigenvalues, and the eigenfunctions are determined from

$$\frac{d}{ds}\left[\phi\frac{df}{ds}\right] = -\varepsilon f \tag{22}$$

where $\tilde{\varepsilon}$ in (21) can be determined from the eigenvalues ε computed from (22) using $\tilde{\varepsilon} = \alpha\varepsilon$.

For a general function ϕ it is necessary to determine the set of eigenfunctions and eigenvalues associated with equation (22) numerically. (Analytical properties of eigenfunctions and details of numerical methods to solve eigenfunction problems are given by Wilkinson.[12]) In order to ensure consistency with the numerical approach used to solve the hydrodynamic equations, the Galerkin method is used to calculate the eigenfunctions of (22).

Thus, expanding the rth eigenfunction f_r in terms of a set of $\bar{m}$ coefficients d_{ir} and basis functions M_i, gives

$$f_r = \sum_{i=1}^{\bar{m}} d_{ir} M_i(s) \tag{23}$$

Applying the Galerkin method to (22), the rth eigenfunction equation is multiplied by f_k and integrated over the region 0 to 1, giving

$$\int_0^1 \frac{\mathrm{d}}{\mathrm{d}s}\left[\phi \frac{\mathrm{d}f_r}{\mathrm{d}s}\right] f_k \,\mathrm{d}s = -\varepsilon_r \int_0^1 f_r f_k \,\mathrm{d}s, \qquad k = 1, 2, \ldots, \bar{m} \tag{24}$$

For an arbitrary ϕ the eigenvalues and eigenfunctions given by (24) may be complex. However, if (24) is integrated by parts, we obtain,

$$\phi \frac{\mathrm{d}f_r}{\mathrm{d}s} f_k \Big|_1 - \phi \frac{\mathrm{d}f_r}{\mathrm{d}s} f_k \Big|_0 - \int_0^1 \phi \frac{\mathrm{d}f_r}{\mathrm{d}s} \frac{\mathrm{d}f_k}{\mathrm{d}s} \,\mathrm{d}s = -\varepsilon_r \int_0^1 f_r f_k \,\mathrm{d}s \tag{25}$$

It can be readily shown that the eigenvalues and eigenvectors determined by the solution of (25) will be real, provided,

$$\phi \frac{\mathrm{d}f_r}{\mathrm{d}s} f_k \Big|_0 = 0 \tag{26a}$$

$$\phi \frac{\mathrm{d}f_r}{\mathrm{d}s} f_k \Big|_1 = 0 \tag{26b}$$

Using (26), equation (25) simplifies to

$$\int_0^1 \phi \frac{\mathrm{d}f_r}{\mathrm{d}s} \frac{\mathrm{d}f_k}{\mathrm{d}s} \,\mathrm{d}s = \varepsilon_r \int_0^1 f_r f_k \,\mathrm{d}s, \qquad k = 1, 2, \ldots, m \tag{27}$$

For convenience the eigenfunctions are normalized by requiring that $f_r(0) = 1$ for all r.

Condition (26a, b) means that in the general case in which the eddy viscosity is non-zero at the sea surface and sea bed, $\mathrm{d}f_r(0)/\mathrm{d}s$ or $f_r(0)$ must be zero. The corresponding condition at the sea bed is that $\mathrm{d}f_r(1)/\mathrm{d}s$ or $f_r(1)$ is zero for all r.

In practice we do not want $f_r(0) = 0$ (for all r) since this forces the u and v components of surface current, evaluated from expansions (9) and (10) to be zero, a condition which is not physically realistic in the problems considered later in this paper. However if $f_r(0) \neq 0$ then eigenfunctions computed from (27) will have $\mathrm{d}f_r(0)/\mathrm{d}s = 0$ because of condition (26a). Such a condition is physically acceptable since external surface stresses are included explicitly in the equations of motion (see equation (19)) by using the Galerkin method. The condition $\mathrm{d}f_r(0)/\mathrm{d}s = 0$ is in fact a necessary surface boundary condition for tidal flow. However in the next section it will be shown that setting $\mathrm{d}f_r/\mathrm{d}s(0) = 0$ does affect the convergence of expansions (9) and (10) for problems involving wind induced motion.

With a no-slip condition at the sea bed, $f_r(1) = 0$ is an essential boundary condition and is the physically correct condition to use at the sea bed. However for the case of a slip bottom

condition $f_r(1) \neq 0$ and consequently eigenfunctions computed from (27) will have $df_r(1)/ds = 0$, for all r, because of condition (26b).

Substituting expansion (23) into (27) and writing (27) in matrix form gives

$$\mathbf{d}^T\mathbf{D}\mathbf{d} = \boldsymbol{\varepsilon}\mathbf{d}^T\mathbf{C}\mathbf{d} \tag{28}$$

where $\mathbf{d}$ is the matrix of coefficients

$$\begin{bmatrix} d_{11} & d_{12} & \cdots & d_{1\bar{m}} \\ d_{21} & \cdots & \cdots & \vdots \\ \vdots & & & \vdots \\ \vdots & & & \vdots \\ d_{\bar{m}1} & & & d_{\bar{m}\bar{m}} \end{bmatrix}$$

and d^T is its transpose. $\boldsymbol{\varepsilon}$ is the diagonal matrix of eigenvalues

$$\begin{bmatrix} \varepsilon_1 & 0 & \cdots & 0 \\ 0 & \varepsilon_2 & \cdots & 0 \\ \vdots & & & \vdots \\ \vdots & & & \vdots \\ 0 & \cdots & \cdots & \varepsilon_{\bar{m}} \end{bmatrix}$$

$\mathbf{D}$ is the matrix of integrals

$$\begin{bmatrix} \int_0^1 \phi M_1' M_1' \, ds & \cdots & \int_0^1 \phi M_1' M_{\bar{m}}' \, ds \\ \vdots & & \vdots \\ \vdots & & \vdots \\ \int_0^1 \phi M_{\bar{m}}' M_1' \, ds & \cdots & \int_0^1 \phi M_{\bar{m}}' M_{\bar{m}}' \, ds \end{bmatrix}$$

and $\mathbf{C}$ is the matrix of integrals

$$\begin{bmatrix} \int_0^1 M_1 M_1 \, ds & \cdots & \int_0^1 M_1 M_{\bar{m}} \, ds \\ \vdots & & \\ \int_0^1 M_{\bar{m}} M_1 \, ds & \cdots & \int_0^1 M_{\bar{m}} M_{\bar{m}} \, ds \end{bmatrix}$$

where $M_i' = dM_i/ds$

Equation (28) is in the standard form of an eigenvalue problem which can be solved using any one of the numerous numerical methods which exists in the literature. In practice the eigenvalue problem was solved using Householder reduction and the QL algorithm.[13]

(ii) *Formulation using eigenfunctions.* For the case in which the basis functions f_r are eigenfunction determined by (27), equation (19) can be further simplified, by taking advantage of the fact that the eigenfunctions are orthogonal,

$$\int_0^1 f_r f_k \, ds = 0, \qquad r \neq k \tag{29}$$

and can be normalized such that

$$f_r(0) = 1, \qquad r = 1, 2, \ldots, m \tag{30}$$

Hence using (29), (27) and condition (30), equation (19) reduces to

$$\frac{\partial A_k}{\partial t}\int_0^1 f_k f_k \, ds = \gamma B_k \int_0^1 f_k f_k \, ds - g\frac{\partial \zeta}{\partial x}\int_0^1 f_k \, ds$$
$$-\frac{F_B}{\rho h} f_k(1) + \frac{F_s}{\rho h} - \alpha \frac{\varepsilon_k}{h^2} A_k \int_0^1 f_k f_k \, ds, \qquad k = 1, 2, \ldots, m \tag{31}$$

In practice it is convenient to write expansions (9) and (10) in the form

$$u = \sum_{r=1}^{m} A_r f_r = \sum_{r=1}^{m} u_r \phi_r f_r \tag{32}$$

$$v = \sum_{r=1}^{m} B_r f_r = \sum_{r=1}^{m} v_r \phi_r f_r \tag{33}$$

where

$$\phi_r = \frac{1}{\int_0^1 f_r f_r \, ds} \tag{34}$$

and u_r, v_r are coefficients varying with horizontal position and time. Using (32) and (33), equation (31) reduces to

$$\frac{\partial u_k}{\partial t} = \gamma v_k - g a_k \frac{\partial \zeta}{\partial x} - \frac{F_B}{\rho h} f_k(1) + \frac{F_s}{\rho h} - \frac{\alpha}{h^2} \varepsilon_k u_k, \qquad k = 1, 2, \ldots, m \tag{35}$$

where

$$a_k = \int_0^1 f_k \, ds$$

Similarly for the v-equation of motion, equation (3), we obtain

$$\frac{\partial v_k}{\partial t} = -\gamma u_k - g a_k \frac{\partial \zeta}{\partial y} - \frac{G_B}{\rho h} f_k(1) + \frac{G_s}{\rho h} - \frac{\alpha}{h^2} \varepsilon_k v_k \tag{36}$$

From equation (12) we obtain the continuity equation,

$$\frac{\partial \zeta}{\partial t} + \sum_{r=1}^{m} \left(\frac{\partial}{\partial x}(h u_r) + \frac{\partial}{\partial y}(h v_r) \right) \phi_r a_r = 0 \tag{37}$$

Once the coefficients d_{ir} in expansion (23), and the eigenvalues ε_r have been computed from (28), the integrals ϕ_r and a_r required in equations (35), (36) and (37) can be readily evaluated.

Equations (35), (36) and (37) are the working equations used to integrate the coefficients u_r, v_r and free surface elevation ζ forward with time.

In order to integrate these equations it is necessary to discretize in the horizontal space domain, and through time. In the numerical calculations presented in the next section of this paper, a staggered finite difference grid was used in the horizontal (see Figure 1). Details of this grid, and methods used to discretize in the horizontal, equations analogous to (35), (36) and (37) have been given previously.[2,4]

Using equations (35), (36) and (37) starting from an initial state of rest in which $\zeta, \{u_r\}, \{v_r\}$ are zero, the solution for the free surface elevation ζ, and the coefficients u_r and v_r may be advanced through time. Currents at any depth and time can then be computed from the coefficients u_r, v_r using expansions (32) and (33).

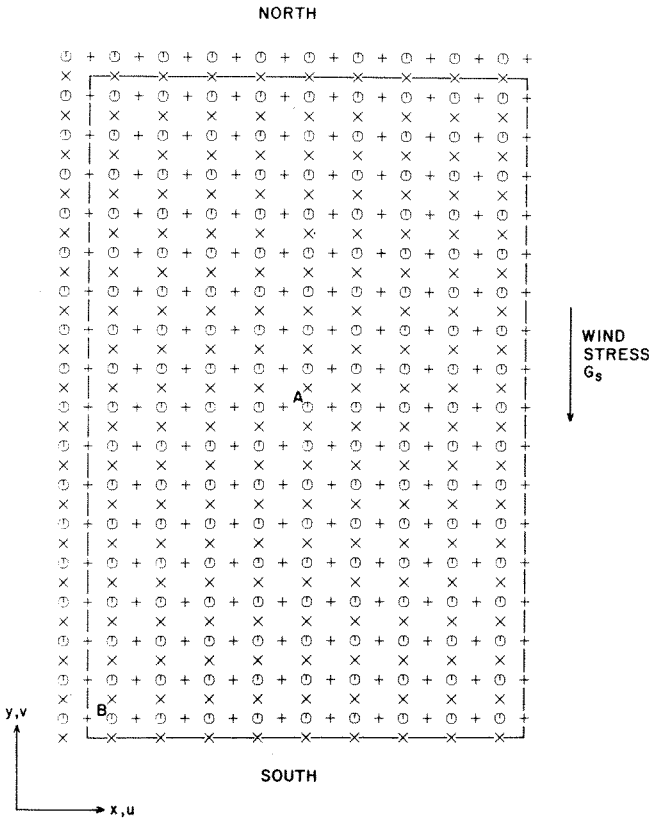

Figure 1. Finite difference grid over the rectangular basin, ○ a ζ-point, + a u-point, × a v-point, —land boundary

(d) *Form of the basis functions used to compute the eigenfunctions*

Considering now the basis function M_i, employed to calculate the eigenfunctions f_i. In theory the choice of functions M_i, is arbitrary, however for the problems considered later (see Section 3) it is advantageous to use piecewise functions, so that increased resolution in the boundary layers, near the sea surface and sea bed can be obtained. Davies[14] has shown that accurate solutions of partial differential equations can be obtained with a basis set of fourth order B-splines, and for this reason these functions are employed here to calculate the eigenfunctions f_i.

B-splines are piecewise polynomials, which are non-zero only over a finite interval of space (Figure 2). Points along the s axis, at which the B-spline changes from a zero to a non-zero function are termed knots, denoted by λ_i. A fourth order B-spline M_i is non-zero only over the interval $\lambda_{i-4} \leqslant s \leqslant \lambda_i$, and at the points λ_{i-4} and λ_i, M_i and its derivatives vanish.

Figure 2 shows the interval from sea surface to sea bed, $0 \leqslant s \leqslant 1$, divided into ten interior knot segments. The number of B-splines in this interval can be readily increased by increasing the number of knots. The position of the knots and their separation is arbitrary, hence resolution in any area can be increased by increasing the number of knots and decreasing their separation in the region where higher resolution is required.

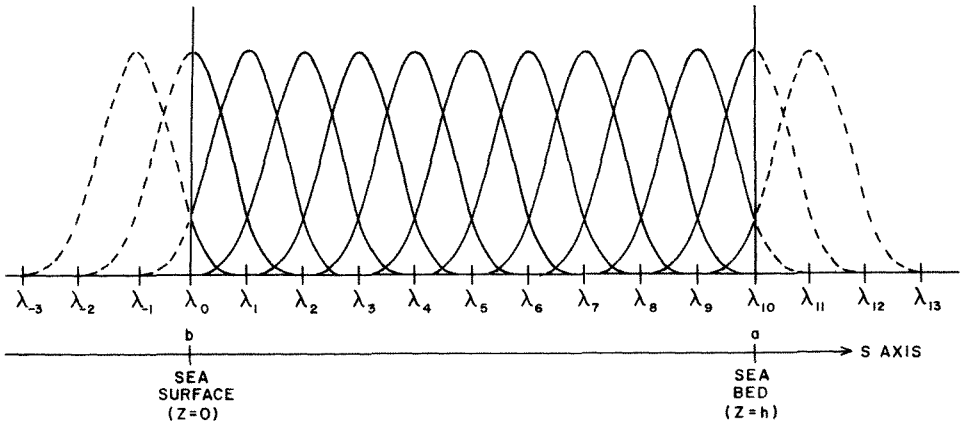

Figure 2. Distribution of B-splines and associated knots with depth

The numerical methods used to generate the B-splines, and to evaluate the integrals which arise in equation (28) have been described in detail by Davies[14] and will not be repeated here.

For the case of stress surface and bottom conditions, *natural* boundary conditions, it is not necessary for each of the basis functions f_r to satisfy these boundary conditions exactly and consequently expansion (23) can be used directly in the eigenvalue problem given by equation (27).

However for the case in which a no slip bottom boundary condition is employed (an *essential* boundary condition) it is necessary for each basis function f_r to satisfy this boundary condition exactly. Consequently,

$$f_r(1) = 0 \quad \text{for all } r \tag{38}$$

In order to satisfy this condition, it is necessary for

$$f_r(1) = \sum_{i=1}^{\bar{m}} d_{i,r} M_i(1) = 0 \tag{39}$$

Owing to the piecewise nature of the B-splines, for the case of fourth order B-splines, (39) reduces to

$$d_{\bar{m}-2,r} W_{\bar{m}-2} + d_{\bar{m}-1,r} W_{\bar{m}-1} + d_{\bar{m},r} W_{\bar{m}} = 0 \tag{40}$$

where

$$W_i = M_i(1)$$

Incorporating condition (39) into expansion (23) gives

$$f_r = \sum_{i=1}^{\bar{m}-3} d_{i,r} M_i + d_{\bar{m}-2;r} \bar{M}_{\bar{m}-2} + d_{\bar{m}-1,r} \bar{M}_{\bar{m}-1}(s) \tag{41}$$

where

$$\bar{M}_{\bar{m}-2} = M_{\bar{m}-2} - \frac{W_{\bar{m}-2}}{W_{\bar{m}}} M_{\bar{m}}, \qquad \bar{M}_{\bar{m}-2} = \bar{M}_{\bar{m}-1} - \frac{W_{\bar{m}-1}}{W_{\bar{m}}} M_{\bar{m}}$$

Thus, expansion (41) satisfies the no-slip boundary condition ($f_r(1) = 0$, $r = 1, 2, \ldots, \bar{m}$) for all coefficients $d_{i,r}$, by introducing modified B-splines $\bar{M}_{\bar{m}-2}$ and $\bar{M}_{\bar{m}-1}$ into the expansions.

3. NUMERICAL CALCULATIONS

(a) *Calculation of eigenfunctions using an expansion of B-splines*

Before considering the solution of the hydrodynamic equations using expansions of eigenfunctions, it is instructive to examine the rate of convergence of expansion (23) for a few idealized vertical variations of N, for which analytical solutions are available.

Case (i). $N = constant$, $f_r'(0) = 0$, $f_r'(1) = 0$, and normalizing condition $f_r(0) = 1$. In this particular case $\phi = 1$ and $\alpha(x, y, t) = N$. Solution of eigenvalue problem (22) is

$$f_r = \cos \alpha_r s; \qquad \varepsilon_r = \alpha_r^2 \tag{42}$$

where

$$\alpha_r = r\pi \qquad r = 0, 1, 2, \ldots, \infty$$

The eigenfunctions f_r are the well known cosine functions and are independent of N.

The first five eigenvalues ε_r computed using an increasing number of uniformly spaced interior knots $\bar{M}$, are given in Table I, together with values computed analytically. (The number of splines $\bar{m}$ used in expansion (23) is given by $\bar{m} = \bar{M} + n - 1$, where n is the order of the B-spline, which in these calculations was four). It is evident from this table that the eigenvalues computed using expansions of B-splines rapidly converge to those determined analytically. From Table I, it is apparent that with an expansion of B-splines, using ten interior knots, ($\bar{M} = 10$), the first three eigenvalues can be computed to an accuracy of 0·0001, although in order to obtain this degree of accuracy for ε_5 it is necessary to increase the number of interior knots to twenty (i.e. $\bar{M} = 20$).

Table I. Eigenvalues computed using an increasing number of internal knot intervals $\bar{M}$, for the case of a slip bottom boundary condition.

Eigenvalues	Number of internal knots $\bar{M}$ 10	15	20	Analytical solution
ε_1	0·0000	0·0000	0·0000	0·0000
ε_2	9·8696	9·8696	9·8696	9·8696
ε_3	39·4785	39·4785	39·4784	39·4784
ε_4	88·8292	88·8262	88·8263	88·8264
ε_5	159·9477	157·9153	157·9138	157·9137

Case (ii). $N = constant$, $f_r'(0) = 0$, $f_r(1) = 0$ and normalizing condition $f_r(0) = 1$. This case corresponds to a no-slip bottom boundary condition, i.e. an essential boundary condition, for which $f_r(1) = 0$ for all r. The solution of the eigenvalue problem (22) is again

$$f_r = \cos \alpha_r s, \qquad \varepsilon_r = \alpha_r^2, \tag{43}$$

but in this case

$$\alpha_r = r\frac{\pi}{2}, \qquad r = 1, 3, 5, \ldots, \infty$$

Comparison of analytical and numerical values of eigenvalues showed as in the previous case, that for a given $\bar{M}$, the error in the computed eigenvalue increases as r increases. However, the error can be reduced if $\bar{M}$ is increased.

(b) *Calculation of wind induced motion in a rectangular basin*

In order to compare the accuracy of current profiles computed using expansions of eigenfunctions, with current profiles computed previously,[2,4] wind induced motion in a simple rectangular sea was examined.

The closed rectangular basin (see Figure 1) has dimensions and rotation representative of the North Sea. Motion in the basin was started from a state of rest by the sudden imposition of a uniform northerly wind stress of -15 dyn/cm^2 (i.e. $F_s = 0$, $G_s = -15$ dyn/cm^2). Other parameters used in the calculation are: $\Delta x = 400/9$ km, $\Delta y = 800/17$ km, $h = 65$ m, $\gamma = 0{\cdot}44\ h^{-1}$, $\rho = 1{\cdot}025$ gm/cm^3, $g = 981$ cm^2/S. These parameters are identical to those used by Davies and Owen[4] in a series of calculations in which wind induced motion in the basin was calculated using a basis set of Chebyshev and Legendre polynomials, and by Davies[2] with a basis set of cosine functions. By repeating these previous calculations, rigorous comparisons between the convergence of expansions of eigenfunctions and rates of convergence found with other basis functions can be made.

In an initial series of computations (calculation (a)), a slip bottom boundary condition was used, with $k = 0{\cdot}2$ cm/s, and N constant at 650 cm^2/s ($0{\cdot}0650$ m^2/s).

Calculation (a): Slip boundary condition $N = 650$ cm^2/s, $k = 0{\cdot}2$ cm/s. It is evident from Table I that the eigenvalues corresponding to the first few eigenfunctions can be accurately computed with $\bar{M} = 20$.

In order to examine the convergence of expansions of these eigenfunctions, surface and bottom u and v components of current, at the centre of the basin (point A, in Figure 1), thirty hours after the onset of the wind field are given in Table II. For comparision purposes, currents evaluated using expansions of 10 cosine functions[2] and 20 cosine functions are given together with values computed using 10 Chebyshev and 10 Legendre polynomials.

It is obvious from Table II, that there are no significant differences between currents computed using an expansion of eigenfunctions with $m = 10$ and $m = 20$, and those computed using ten and twenty cosines.[2] In this particular example the cosine functions are the exact eigenfunctions of the problem, and although from Table I, it is obvious that the numerically determined eigenfunctions and eigenvalues are not identical to the cosine function, the inaccuracies in the computed eigenfunctions and eigenvalues do not affect the computed currents.

It is apparent from Table II, that the expansion converges as m, the number of eigenfunctions increases. However in the case of the v component of current at the sea surface this convergence is slow. There is an appreciable difference between the surface v component of current computed using eigenfunctions and that computed using either Chebyshev or Legendre polynomials.[4] This component of current is in the direction of the surface wind stress.

Table II. u and v components of current computed with a slip bottom boundary condition, 30 hours after the onset of the wind field, evaluated using an increasing number of eigenfunctions (m).

Depth	Component of current (cm/s)	Number of eigenfunctions m 5	10	15	20	10 Cosines	20 Cosines	10 Chebyshev	10 Legendre
Surface	u	−14·90	−14·92	−15·00	−15·01	−14·92	−15·00	−15·06	−15·12
	v	−27·09	−30·11	−31·21	−31·69	−30·11	−31·68	−33·20	−33·20
Sea bed	u	7·40	7·11	7·08	7·04	7·11	7·04	6·96	7·07
	v	12·20	12·47	12·22	12·23	12·47	12·24	12·07	11·75

Table III. u and v components of current, computed with a slip bottom boundary condition, 30 hours after the onset of the wind field, evaluated using a basis set of B-splines.

Depth	Component of current (cm/s)	Number of internal knots $\bar{M}$ 2	4	6	8	10
Surface	u	−14·91	−15·06	−15·06	−15·06	−15·06
	v	−33·31	−33·15	−33·15	−33·15	−33·15
Sea bed	u	7·05	6·95	6·95	6·95	6·95
	v	12·00	12·08	12·08	12·08	12·08

The poor convergence of the expansion for the v component of current at the sea surface, has been shown to arise[2] because the derivative of the cosine functions and also the numerically derived eigenfunctions, at the sea surface are zero. Consequently the surface stress computed with a finite number of cosine functions or numerically derived eigenfunctions will always be zero. Hence the expansions cannot convergence with a finite number of terms to the externally applied wind stress.

In the case of the u-component of current, the wind stress at the surface is zero. A surface condition which is automatically satisfies by the functions. In this case the expansions converge rapidly for all depths.

An alternative to using an expansion of B-splines to compute eigenfunctions, and then using these eigenfunctions as a basis set for the solution of the hydrodynamic equations is to use the B-splines directly as basis functions. This approach has been used previously[9] to solve the hydrodynamic equations. However, Davies[9] did not include the surface stress condition as a natural boundary condition, but satisfied it exactly by linearly combining the spline functions. It is therefore particularly interesting to compute currents using an expansion of B-splines, in which the surface stress condition is included as a natural boundary condition. Currents computed by this method can then be compared with currents determined using eigenfunction expansions, and rates of convergence examined. In both cases surface and bottom boundary conditions are treated as natural boundary conditions.

Currents at sea surface and sea bed, computed using B-splines, with an increasing number of interior knots $\bar{M}$, are given in Table III. Referring to this Table, it is evident that the B-spline expansion rapidly converges. Surface and bottom currents computed with $\bar{M}=4$ agreeing to within 0·05 cm/s with those computed using an expansion of ten Chebyshev polynomials. Obviously in this particular example, the eigenfunctions, computed from equation (22) are not the optimum functions (in the sense that an expansion of them converges more rapidly than expansion of any other function), to use as a basis set.

Calculation (b): No slip boundary condition, N varying in a linear manner through the vertical. In the previous example a slip bottom boundary condition was used, with a constant value of eddy viscosity. We now consider the case in which a no slip bottom boundary condition is employed, with a vertically varying eddy viscosity (Distribution A in Figure 3). Referring to this Figure, the total depth of the water was 65 m, with d_1 and d_3 fixed at 11 m, approximating a surface and a bottom boundary layer, within which N varied linearly. In order to compare currents computed using a basis set of eigenfunctions with those computed using Chebyshev or Legendre polynomials[4] or cosine functions,[2] identical values of N_s, N_m, N_h, to those used previously, were employed, namely $N_s = 130$ cm^2/s, (0·0130 m^2/s) $N_m = 650$ cm^2/s, (0·0650 cm^2/s), $N_h = 130$ cm^2/s (0·0130 m^2/s).

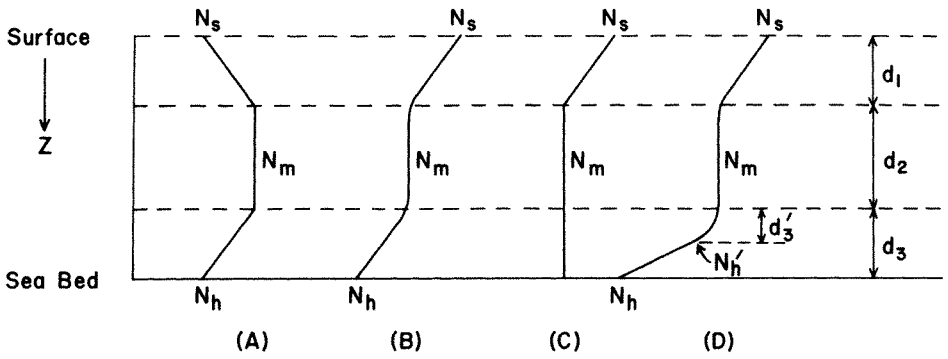

Figure 3. Schematic diagram showing the various depth distributions (A), (B), (C) and (D) of eddy viscosity used in the calculations

In this particular example, N did not vary with horizontal position or time, consequently $\alpha(x, y, t) = 1{\cdot}0$ in equations (31) and (36). The functional form of ϕ used in equation (22) is given schematically by Distribution A in Figure 3, with values of N_s, N_m, N_h as stated. The values of ε_i together with the corresponding f_i used in equations (31) and (36) are determined by the solution of (22).

Currents at sea surface and mid-depth, computed using a basis set of eigenfunctions, derived from this eddy viscosity distribution, are given in Table IV. The eigenfunctions were determined using an expansion of B-splines, with twenty five uniformly spaced interior knots (i.e. $\bar{M} = 25$).

It is apparent from this Table that the eigenfunction expansion converges rapidly at all depths, except for the surface v-component of current. For comparison purposes, currents computed using a basis set of cosine functions, given by equation (43), taken from Reference 2 are also given. Comparing currents computed using these two different basis sets, it is evident that there is a significant improvement in convergence using eigenfunctions rather than cosine functions, particularly for the V-component of surface current.

In order to understand why the expansion of eigenfunctions converges faster at the sea surface, than an expansion of cosine functions, it is necessary to examine the vertical variation of these functions. The first five eigenfunctions are plotted as a function of the vertical co-ordinate in Figure 4(a). From this Figure it is apparent that the oscillatory nature of the eigenfunctions increases as r increases. This is a necessary requirement for orthogonal functions. Each eigenfunction has a steep gradient near the sea surface, which increases with r. This steep gradient enables them to accurately model the high shear surface layer which occurs when a wind stress is applied at the water's surface. The existence of this region of rapid change in the higher eigenfunctions, and the absence of such a region in the cosine

Table IV. u and v components of current, computed with a no-slip bottom boundary condition, 15 hours after the onset of the wind field, evaluated using basis sets of eigenfunctions and cosines

Component cm/s	Depth s	Number of eigenfunctions 5	10	15	20	25	Number of cosine functions 5	10	15	20	25
u	0·0	−11·98	−12·22	−12·13	−12·14	−12·14	−9·0	−11·4	−11·8	−12·0	−12·1
	0·5	3·42	3·46	3·46	3·46	3·46	3·4	3·6	3·5	3·5	3·5
v	0·0	−27·04	−34·25	−36·66	−37·59	−37·95	−16·0	−26·6	−30·7	−33·5	−35·0
	0·5	19·54	20·69	20·88	20·76	20·72	19·3	20·7	20·7	20·7	20·7

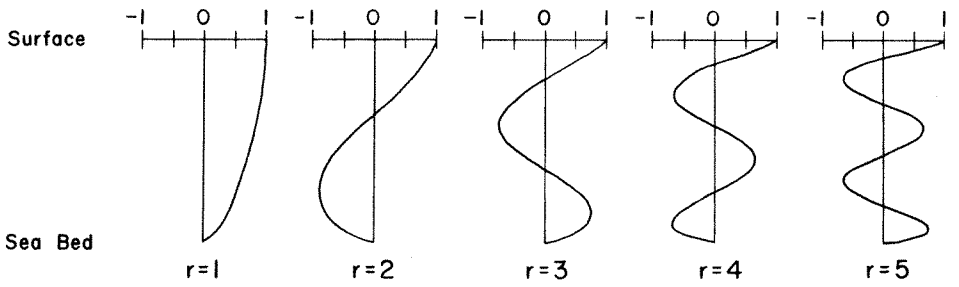

Figure 4(a). Vertical variation of the first five eigenfunctions computed numerically with knot distribution F (Table VI) and eddy viscosity profile A (Figure 3), with $N_s = 130\,\text{cm}^2/\text{s}$, $N_m = 650\,\text{cm}^2/\text{s}$, $N_h = 130\,\text{cm}^2/\text{s}$

functions, explains the improved rate of convergence of the eigenfunctions compared with the cosine functions. A close inspection of Figure 4(a) does however reveal that, just at the sea surface, the shear layer decreases, and the vertical derivative of the eigenfunction tends to zero. This abrupt change in the derivative of the eigenfunction at the sea surface, arises because condition (26a) requires that the derivative of the eigenfunction is zero at the sea surface for the case in which N and $f_r(0)$ are non-zero at the sea surface. The use of a zero stress surface condition obviously affects the convergence of the eigenfunctions at the sea surface. This poor convergence is confirmed by comparing currents given in Table IV with currents computed using an increasing number of B-splines (Table V) as basis functions.

From this comparison it is evident that apart from the surface v component of current, no significant differences (i.e. differences greater than 0·1 cm/s) occur between currents computed using ten eigenfunctions, and those computed using B-splines with $\bar{M} = 8$.

Table V. u and v components of current, computed with a no-slip bottom boundary condition, 15 hours after onset of the wind field, evaluated with a basis set of B-splines

Component cm/s	Depth s	Number of internal knots $\bar{M}$ 2	4	6	8	10
u	0·0	−12·25	−12·38	−12·25	−12·17	−12·15
	0·5	3·51	3·53	3·50	3·47	3·48
v	0·0	−38·27	−40·76	−41·47	−41·56	−41·61
	0·5	17·58	20·74	20·55	20·70	20·72

Calculation (c): No slip bottom boundary, physically realistic vertical variation of N. An appropriate value of eddy viscosity to use in a wind driven problem is at present difficult to determine from the scientific literature. Munk and Anderson[15] have suggested that the value of eddy viscosity at the sea surface should depend upon the wind speed and decrease with depth below the surface. For the wind stress used here a surface value of $N_s = 2600\,\text{cm}^2/\text{s}$ ($0{\cdot}2600\,\text{m}^2/\text{s}$) would appear appropriate.[15] Turbulence below this surface layer is probably dominated by the tidal currents. For tidally induced turbulence Davies and Furnes[11] have proposed that, away from the bottom boundary layer

$$N = \frac{\kappa(\bar{u}^2 + \bar{v}^2)}{\sigma}, \tag{44}$$

where $\sigma = 10^{-4}\,\text{s}^{-1}$, a typical frequency associated with long wave motion, and $\kappa = 2{\cdot}0 \times 10^{-5}$, a dimensionless coefficient.

In (44), $\bar{u}$ and $\bar{v}$ denote depth mean tidal currents, given by

$$\bar{u} = \sum_{r=1}^{m} u_r \phi_r a_r, \qquad \bar{v} = \sum_{r=1}^{m} v_r \phi_r a_r$$

where

$$a_r = \int_0^1 f_r \, \mathrm{d}s$$

In physically realistic models[11,16] N varied with x, y, t according to (44). Such a variation can be included in the present formulation by making α in equations (31) and (36) proportional to $(\bar{u}^2 + \bar{v}^2)$. However, since the present model represents the North Sea by a closed basin it is not possible to include the tide directly in the model. The effect of a mean tidal current upon the value of N_m used in the model can be taken into account using (44) with average values for the amplitudes of the tidal currents. This is consistent with the idealized model used here and yields a fully linear model.

Typically over the North Sea, depth mean tidal currents are on average of the order of 50 cm/s to 60 cm/s. Using these values in equation (44) gives N_m varying from 500 cm^2/s to 720 cm^2/s. In order to make comparisons with previous calculations a value of $N_m =$ 650 cm^2/s was in fact used.

Values of eddy viscosity in the bottom boundary layer are difficult to determine. Heaps and Jones[10] in a numerical calculation of the M_2 tide in the Irish Sea, assumed that N at $z = h$ was given by

$$N_h = Z_0 k_0 K (\bar{u}^2 + \bar{v}^2)^{1/2} \tag{45}$$

where Z_0 is the roughness length, k_0 Von Karman's constant, taken as 0·41, and K the coefficient of bottom friction as defined previously.

From observations, Channon and Hamilton[17] found a range of values of Z_0, typically from 7·0 cm to 0·44 cm. Using equation (45) with these values of Z_0 and a typical tidal current of amplitude 60 cm/s, with $K = 0{\cdot}005$ (Reference 11), gives values of N at the sea bed ranging from 12·2 cm^2/s to 0·8 cm^2/s.

In order to examine the sensitivity of current profiles to changes in Z_0 a series of calculations were performed in which the eddy viscosity at the sea bed took a series of values ranging from 10 cm^2/s to 1 cm^2/s (i.e. approximately covering the observed range). A calculation with $N_h = 130$ cm^2/s was also performed for comparison with earlier calculations. As in the previous calculation, wind induced motion in the rectangular basin was computed, with a no slip bottom boundary condition. However, a smooth continuous physically realistic vertical variation of viscosity was used in these calculations (Distribution B in Figure 3), with N_s, N_m, N_h denoting respectively surface, mid-depth and bottom viscosity. As previously the total depth h was 65 m, with d_1 and d_3 fixed at 11 m, approximating a surface and bottom layer.

In these calculations N_s was fixed at 2600 cm^2/s, N_m at 650 cm^2/s and N_h took a range of values, namely $N_h = 130$, 10, 5, 1 cm^2/s. Since N in these calculations did not vary with horizontal position or time $\alpha = 1.0$ in equations (31) and (36) and the eigenvalues ε_r and eigenfunctions f_r were calculated from (22), with ϕ as shown in distribution B (Figure 3) with appropriate values of N_s, N_m, N_h in m^2/s.

Calculation c(i): $N_s = 2600$ cm^2/s, $N_m = 650$ cm^2/s, $N_h = 130$ cm^2/s. In order to determine the convergence of the expansion of B-splines, eigenfunctions for this eddy viscosity

Table VI. Various knot distributions used in the numerical calculations

Knot distribution	Knot spacing from sea surface $S = 0{\cdot}0$ to sea bed $S = 1{\cdot}0$
A($\bar{M} = 25$)	0·0 (0·04) 1·0
B($\bar{M} = 28$)	0·0 (0·1) 0·5 (0·05) 0·8 (0·02) 0·92 (0·01) 0·97 (0·005) 1·0
C($\bar{M} = 36$)	0·0 (0·04) 0·84 (0·02) 0·92 (0·01) 0·97 (0·005) 1·0
D($\bar{M} = 32$)	0·0 (0·1) 0·5 (0·05) 0·8 (0·02) 0·92 (0·01) 0·97 (0·005) 0·98 (0·0025) 1·0
E($\bar{M} = 34$)	0·0 (0·1) 0·7 (0·05) 0·8 (0·04) 0·84 (0·02) 0·94 (0·01) 0·97 (0·005) 0·985 (0·001) 0·987 (0·0005) 0·990 (0·0025) 0·995 (0·001) 1·0
F($\bar{M} = 37$)	0·0 (0·1) 0·7 (0·005) 0·8 (0·02) 0·94 (0·01) 0·95 (0·005) 0·97 (0·002) 1·00
G($\bar{M} = 37$)	0·0 (0·1) 0·7 (0·05) 0·8 (0·04) 0·86 (0·02) 0·96 (0·01) 0·97 (0·005) 0·990 (0·0025) 0·995 (0·001) 0·997 (0·0005) 1·00

distribution were computed with knot distribution A ($\bar{M} = 25$) and knot distribution B ($\bar{M} = 28$) (see Table VI for the vertical position of knots). From Table VI, it is apparent that distribution (A) is a uniform knot spacing through the vertical, whereas in distribution (B), the knot spacing decreases rapidly near the sea bed.

The convergence of the computed current profiles calculated with both these knot distributions was examined by increasing the number of eigenfunctions used in expansions (9) and (10). Thus m took a range of values, namely $m = 5, 10, 15$.

In Table VII, u and v components of current are given at various normalized depths s, computed using a basis set of eigenfunctions derived with knot distributions (A) and (B) for various values of m.

It is evident from this Table that for both distributions A ($\bar{M} = 25$) and B ($\bar{M} = 28$) the expansions of eigenfunctions converge rapidly. Although there are some slight differences

Table VII. u and v components of current evaluated with $N_s = 0{\cdot}2600\ m^2/s$, $N_m = 0{\cdot}0650\ m^2/s$, $N_h = 0{\cdot}0130\ m^2/s$, using an increasing number of eigenfunctions, which have been computed with knot distributions A and B.

		Eigenfunctions computed with knot distribution A Number of eigenfunctions			Eigenfunctions computed with knot distribution B Number of eigenfunctions		
	S	5	10	15	5	10	15
u (cm/s)	0·0	−7·19	−7·20	−7·21	−7·15	−7·16	−7·17
	0·5	2·60	2·62	2·62	2·59	2·61	2·61
	0·75	4·84	4·84	4·84	4·83	4·83	4·83
	0·95	2·19	2·14	2·14	2·19	2·13	2·14
	0·98	1·09	1·04	1·02	1·08	1·03	1·01
v (cm/s)	0·0	−7·76	−9·13	−9·65	−7·67	−9·05	−9·86
	0·5	18·83	18·86	18·85	18·82	18·97	19·02
	0·75	20·25	19·75	19·76	20·25	19·74	19·80
	0·95	9·19	9·85	9·85	9·19	9·82	9·80
	0·98	4.58	5·16	4·99	4·56	5·09	5·04
ζ (cm)		125·3	125·3	125·3	125·3	125·3	125·3

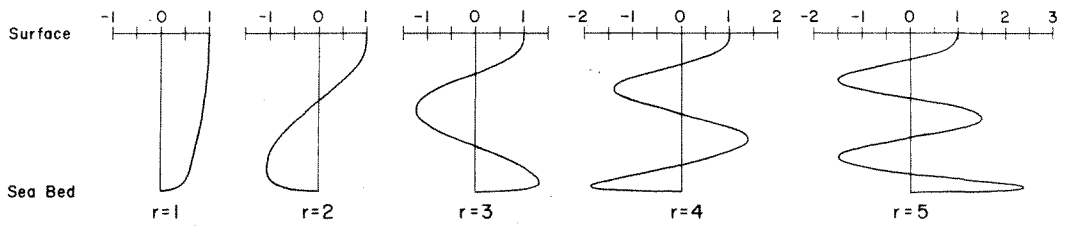

Figure 4(b). Vertical variation of the first five eigenfunctions computed numerically with knot distribution F (Table VI) and eddy viscosity profile B, with $N_s = 2600\ \text{cm}^2/\text{s}$, $N_m = 650\ \text{cm}^2/\text{s}$ and $N_h = 10\ \text{cm}^2/\text{s}$

between current profiles computed with eigenfunctions determined with $\bar{M} = 25$ and $\bar{M} = 28$, these are not significant. However, when this calculation was repeated but with N_h reduced to $10\ \text{cm}^2/\text{s}$, differences in current magnitude, particularly near the sea bed, and in the free surface elevation were evident between the cases computed with an increasing number of eigenfunctions determined numerically using knot distributions (A) ($\bar{M} = 25$) and (B) ($\bar{M} = 28$).

It is apparent from Table VII that the expansion of eigenfunctions converge rapidly, and that current profiles, except for the v component of surface current can be computed to an accuracy of 0·05 cm/s using an expansion of ten eigenfunctions ($m = 10$). However the accuracy of the computed current profile is also determined by the number of B-splines used to compute the eigenfunctions, particularly for the case with $N_h = 10\ \text{cm}^2/\text{s}$.

The importance of using a sufficiently large number of B-splines near the sea bed can be appreciated by examining the vertical variation of the eigenfunctions. The first five eigenfunctions, evaluated numerically with $\bar{M} = 28$, are plotted in Figure 4(b). From this figure it is evident that with $N_h = 10\ \text{cm}^2/\text{s}$ the higher eigenfunctions are characterized by a steep vertical gradient near the sea bed. In order to resolve this gradient it is necessary to ensure that the model has sufficient resolution close to the sea bed. This point will be discussed at length later in this paper.

To examine in more detail the effect upon current profiles of changing the number and distribution of knots and associated B-splines used to compute the basis set of eigenfunctions a series of calculations has been performed. In these calculations the number of eigenfunctions m, used to solve the hydrodynamic equations was fixed at ten. However, the number of B-splines used to compute these eigenfunctions and their associated knot distributions were varied (see Table VI).

Calculation c(ii): $N_s = 2600$, $N_m = 650$, $N_h = 5\ \text{cm}^2/\text{s}$. Current components at point A for various depths s, computed with ten eigenfunctions, determined using various internal knot distributions (given in Table VI) are shown in Table VIII. Also given in the Table is the free surface elevation, at point B, and the first five eigenvalues ε_r.

Referring to Tables VI and VIII, it is evident that the eigenvalues, currents and free surface elevation converge rapidly as the vertical resolution near the sea bed is increased. Comparing current profiles, eigenvalues and free surface elevation computed with distribution A ($\bar{M} = 25$) and distribution B ($\bar{M} = 28$) it is evident that re-distributing the knots through the vertical to increase the resolution near the sea bed enhances the convergence of the solution. A further increase in knots, away from the sea bed (distributions B and C) does not appear to significantly affect the solution, nor in this case does increasing the convergence near the sea bed (compare currents computed with distribution (B) with currents computed with distributions D, E, F and G).

Table VIII. u and v components of current, free surface elevation ζ and eigenvalues ε, evaluated with $N_s = 0{\cdot}2600\ m^2/s$, $N_m = 0{\cdot}0650\ m^2/s$, $N_h = 0{\cdot}0005\ m^2/s$ using ten eigenfunctions computed using various knot distributions. For comparision currents computed using a basis set of B-splines are given.

		Basis set of eigenfunctions Knot distributions							Basis set of splines Knot distributions	
	S	(A)	(B)	(C)	(D)	(E)	(F)	(G)	(B)	(G)
u	0·0	−10·71	−11·22	−11·27	−11·23	−11·24	−11·24	−11·24	−11·23	−11·24
	0·5	1·08	0·79	0·79	0·78	0·78	0·78	0·78	0·78	0·78
	0·75	5·57	5·59	5·60	5·59	5·59	5·59	5·59	5·59	5·59
	0·95	4·57	4·97	4·98	4·97	4·98	4·97	4·98	5·00	4·98
	0·98	3·35	3·74	3·75	3·75	3·75	3·75	3·75	3·74	3·75
v	0·0	−8·64	−8·64	−8·64	−8·64	−8·67	−8·67	−8·67	−10·21	−10·21
	0·5	20·46	20·68	20·59	20·68	20·62	20·62	20·62	20·61	20·60
	0·75	23·64	24·07	24·04	24·08	24·08	24·08	24·08	24·16	24·16
	0·95	17·84	19·14	19·11	19·16	19·16	19·16	19·16	19·26	19·28
	0·98	13·87	15·04	15·07	15·07	15·07	15·07	15·07	14·98	15·01
	ζ	99·72	96·16	96·17	96·10	96·10	96·10	96·10	96·15	96·08
Eigenvalues	ε_1	0·0709	0·0649	0·0649	0·0648	0·0648	0·0648	0·0648	—	—
	ε_2	0·8944	0·8666	0·8660	0·8661	0·8661	0·8661	0·8661	—	—
	ε_3	2·9976	2·9425	2·9367	2·9415	2·9414	2·9414	2·9414	—	—
	ε_4	6·3128	6·1947	6·1759	6·1924	6·1923	6·1923	6·1923	—	—
	ε_5	10·6147	10·4138	10·3707	10·4098	10·4102	10·4103	10·4102	—	—

Comparing eigenfunctions computed with the present distribution of N, with those given in Figure 4(b) it was evident that as N_h is reduced in magnitude the vertical gradient of the eigenfunction at the sea bed increases, and vertical resolution near the sea bed must also increase in order to resolve this region of rapid change.

For comparison purposes currents computed using B-splines as basis functions in the solution of the hydrodynamic equations are given. It is evident that except for the V-component of surface current, no significant differences between currents computed using ten eigenfunctions determined numerically using an expansion of B-splines and those computed solving the hydrodynamic equations with the corresponding basis set of B-splines, were found. However the computer time used to solve the hydrodynamic equations, using eigenfunctions, including calculating the eigenfunctions was an order of magnitude less than that required using a basis set of B-splines based upon distribution (G).

Calculation c (iii): $N_s = 2600$, $N_m = 650$, $N_h = 1\ cm^2/s$

To examine the effect upon the rate of convergence of the splines, of further reducing the value of eddy viscosity at the sea bed, the previous calculation was repeated but with $N_h = 1\ cm^2/s$. It is evident from Table IX that the B-spline expansion used to compute the eigenvalues and associated eigenfunctions converged significantly slower than in the previous example. Also the vertical gradient of the eigenfunction near the sea bed increased rapidly as N_h decreased. It is therefore necessary to increase the resolution near the sea bed as N_h decreases. If insufficient resolution is used, this region is not resolved correctly, and the computed eigenfunctions are not solutions of the eigenvalue problem with $N(z)$ as specified, but are eigenfunctions of an eigenvalue problem involving a perturbed eddy viscosity $\tilde{N}(z)$ which approximates the specified $N(z)$. This can be demonstrated by comparing current profiles, free surface elevation ζ, and eigenvalues computed in Table IX with distribution A ($\bar{M} = 25$), with those computed in Table VIII, with distrubutions (F) or (G) ($\bar{M} = 37$) (an accurate solution of the hydrodynamic equations with $N_s = 2600$, $N_m = 650$, $N_s = 5\ cm^2/s$). It is evident from this comparison that current profiles, free surface elevation, and eigenfunctions computed for $N = 2600$, 650, 1, with $\bar{M} = 25$ correspond with the accurate solution of

Table IX. u and v components of current, free surface elevation ζ and eigenvalues ε, evaluated with $N_s = 0{\cdot}2600\ \mathrm{m^2/s}$, $N_m = 0{\cdot}0650\ \mathrm{m^2/s}$, $N_h = 0{\cdot}0001\ \mathrm{m^2/s}$ using ten eigenfunctions computed using various knot distributions. For comparision currents computed using a basis set of B-splines are given

		Basis set of eigenfunctions Knot distributions							Basis set of B-splines Knot distributions	
		(A)	(B)	(C)	(D)	(E)	(F)	(G)	(B)	(G)
u	0·0	−11·08	−12·25	−12·30	−12·39	−12·45	−12·42	−12·46	−12·26	−12·46
	0·5	0·90	0·26	0·27	0·19	0·16	0·17	0·15	0·26	0·15
	0·75	5·61	5·67	5·69	5·68	5·68	5·68	5·68	5·67	5·68
	0·95	4·83	5·69	5·71	5·79	5·83	5·81	5·83	5·70	5·84
	0·98	3·68	4·67	4·68	4·80	4·85	4·81	4·84	4·68	4·86
v	0·0	−8·60	−8·59	−8·58	−8·58	−8·61	−8·60	−8·61	−10·17	−10·16
	0·5	20·59	20·97	20·89	21·00	20·95	20·94	20·95	20·87	20·91
	0·75	23·97	24·87	24·84	24·96	25·01	24·98	25·01	24·94	25·08
	0·95	18·60	21·15	21·12	21·40	21·51	21·44	21·52	21·27	21·64
	0·98	14·93	17·75	17·76	18·10	18·25	18·16	18·26	17·76	18·27
	ζ	97·39	90·08	90·09	89·28	88·94	89·14	88·90	90·07	88·90
Eigenvalues	ε_1	0·0665	0·0536	0·0536	0·0521	0·0515	0·0519	0·0515	—	—
	ε_2	0·8743	0·8179	0·8173	0·8118	0·8093	0·8108	0·8090	—	—
	ε_3	2·9583	2·8418	2·8364	2·8289	2·8235	2·8267	2·8229	—	—
	ε_4	6·2309	5·9741	5·9568	5·9453	5·9334	5·9405	5·9321	—	—
	ε_5	10·4761	10·0478	10·0075	10·0014	9·9828	9·9941	9·9807	—	—

the hydrodynamic equations with $N = 2600, 650, 5$. This demonstrates that in the case in which $\bar{M} = 25$, the eigenvalues and eigenfunctions are solution of a perturbed eigenvalue problem in which $\tilde{N}(z) \approx 2600, 650, 5$ and not the original distribution of 2600, 650, 1. To summarize, the effect of using an insufficient number of B-splines near the sea bed, means that the high shear in this region is not represented accurately and the vertical gradient of the computed eigenfunctions is underestimated at the sea bed. The physical implication of underestimating the vertical gradient at the sea bed is to artificially increase the value of eddy viscosity at the sea bed. The computed numerical solution therefore no longer corresponds to the true solution of the problem in which the eddy viscosity is given by $N(z)$, but is a solution of the problem in which the vertical variation of N is given by $\tilde{N}(z)$.

It is evident from Tables VIII and IX, that the artificial increase in eddy viscosity at the sea bed which arises when insufficient vertical resolution is used in the calculation, occurs when either a basis set of B-splines or eigenfunctions is used. By using a basis set of eigenfunctions, it is possible to check that there is sufficient vertical resolution by computing the eigenfunctions and eigenvalues with a range of increasing vertical resolutions, i.e. an increasing number of B-splines. Since this check on accuracy can be performed prior to the solution of the hydrodynamic equations, computer time is minimized. Having computed an accurate set of eigenfunctions, a basis set of ten functions appears adequate to solve the hydrodynamic equations.

If the alternative approach of using the B-splines directly to solve the hydrodynamic equations is employed, then it is necessary to solve these equations for a range of vertical resolutions, if a check on the accuracy of the solution is to be made. Naturally this approach will involve a significant amount of computer time. Also, a basis set of the order of thirty to forty B-splines appears necessary when N_h has a low value compared with N_s and N_m. Although when N_h is comparable with N_m, a basis set of B-splines converges more rapidly than a basis set of eigenfunctions as demonstrated previously.

4. COMPARISION OF SEA SURFACE ELEVATIONS AND CURRENT PROFILES COMPUTED USING SLIP AND NO-SLIP BOTTOM BOUNDARY CONDITIONS

It is evident from the previous series of calculations that the free surface elevation and the magnitude of the current computed using a no-slip boundary condition are critically dependent upon the value of eddy viscosity N_h and hence Z_0 at the sea bed.

To examine the effect upon ζ, u and v of changing the value of N_h wind induced motion in the rectangular basin, produced by a suddenly imposed wind stress of 15 dynes/cm^2 was again computed. In these calculations the B-spline distribution F ($\bar{M} = 37$) (Table VII) was used to compute the eigenfunctions, and an expansion of ten of these functions was employed in the solution of the hydrodynamic equations. Eddy viscosity distribution B (Figure 3) was used with surface eddy viscosity N_s fixed at 2600 cm^2/s and $N_m = 650$ cm^2/s. The thickness of the upper layer was $d_1 = 11$ m.

In an initial series of calculations d_2 was fixed at 11 m, and N_h took a range of values, namely $N_h = 1$, 5, 10, 50 cm^2/s. To test the effect of decreasing d_2, a second series of calculations were performed with the same range of values of N_h, but with $d_2 = 7$ m. In order to compare ζ, u and v computed using slip and no-slip bottom boundary conditions, the model was also run with the eddy viscosity distribution C (Figure 3), $N_h = N_m$, but with a slip bottom boundary condition. Referring to this figure, $N_s = 2600$ cm^2/s, $N_m = 650$ cm^2/s.

In a physically realistic model, in which the tides are included,[11,16] bottom stress is computed using the quadratic law of friction (equation 7). In the present idealized model the tides are not included but their effect upon bottom friction can be introduced in the slip model by linearizing equation (7) to give equation (6).

Linearizing bottom friction,[18,19] the resulting coefficient k in equation (6) is given in terms of K [equation (7)] by

$$k = \frac{4KU}{\pi} \tag{46}$$

where U is the amplitude of the tidal velocity. Typical values of K are of the order of 0·002 to 0·005.[11] Taking U to be between 50 cm/s to 60 cm/s, equation (46) gives a range of values of k from 0·127 cm/s to 0·382 cm/s. Linearizing bottom friction in the slip model is consistent with the use of a constant value of eddy viscosity based upon a mean tidal velocity in the no slip model, rather than the non-linear form given by equation (44).

A series of calculations were performed with the slip model in which $k = 0{\cdot}1$ cm/s, 0·2 cm/s, 0·4 cm/s, values covering the range of k from 0·127 cm/s to 0·382 cm/s, given by equation (46).

Since the eddy viscosity in both the slip and no-slip models did not vary with x, y or t, then $\alpha(x, y, t) = 1{\cdot}0$ in equations (31) and (36), with ε_r and f_r calculated from (22), with ϕ as given by distributions B and C (Figure 3).

Sea surface elevations at position B, plotted as a function of time, for various values of N_h are given in Figure 5. In these calculations the thickness of the bottom boundary layer was fixed at $d_2 = 11$ m. For comparison purposes elevations computed using a slip bottom boundary conditions with $k = 0{\cdot}1$ cm/s, 0·2 cm/s and 0·4 cm/s are also shown.

It is evident from this Figure that the damping of the sea surface elevation, following the imposition of the wind field, computed using a no-slip boundary condition, increases as N_h increases. The phase of the peak of the maximum and minimum elevation is also affected, with the wavelength increasing as N_h increases. The magnitude of the mean value of ζ also rises as N_h is increased. The plot of sea surface elevation computed using a no-slip bottom boundary condition with $N_h = 1$ cm/s, was not significantly different from that computed with

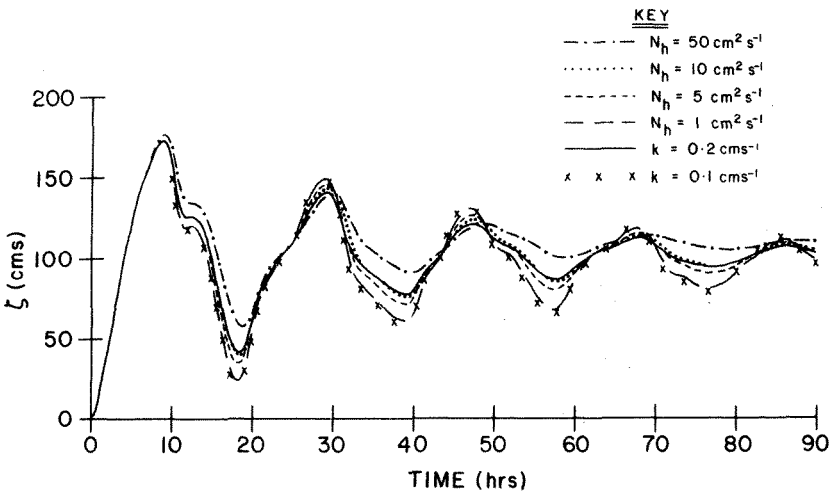

Figure 5. Time series of elevations ζ at corner point B, computed using a no slip model with $d_2 = 11$ m (Figure 3, distribution B), and $N_h = 50$, 10, 5, 1 cm^2/s and a slip model with $k = 0{\cdot}2$, $0{\cdot}1$ cm/s

$k = 0{\cdot}1$ cm/s. Similar agreement occurred in the case in which $N_h = 50$ cm^2/s and $k = 0{\cdot}4$ cm/s. Evidently increasing the value of k has a similar effect upon ζ as increasing N_h.

The effect of decreasing the thickness of the bottom boundary layer from 11 m to 7 m, is to increase the damping of the free surface elevation, compare Figure 6 with Figure 5. It is evident from Figure 6, that the time variation of the free surface elevation computed with $N_h = 1$ cm^2/s and $d_2 = 7$ m, closely resembles that computed using a slip condition with $k = 0{\cdot}2$ cm/s. Comparing in Figures 5 and 6, the time variation of ζ computed with $N_h = 1$ cm^2/s, it is apparent that reducing the thickness of the bottom boundary layer from 11 m to 7 m, with N_h fixed at 1 cm^2/s is to a first order, equivalent to increasing k from

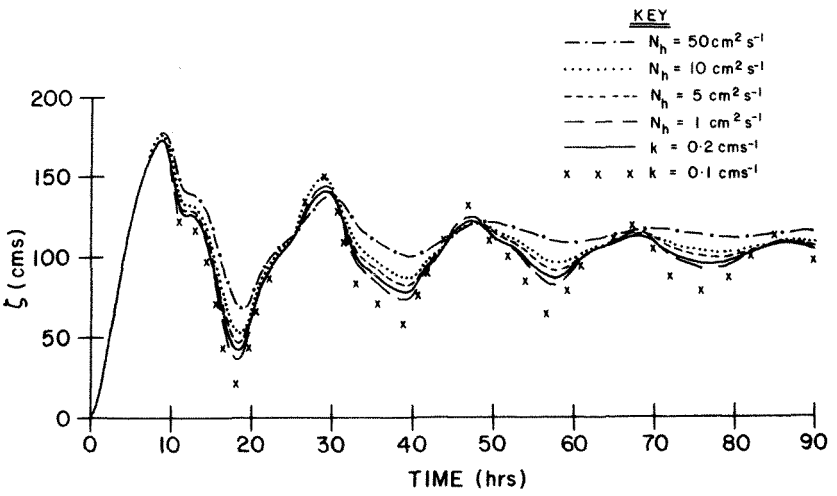

Figure 6. Time series of elevations ζ at corner point B, computed using a no slip model with $d_2 = 7$ m (Figure 3 distribution B), and $N_h = 50$, 10, 5, 1 cm^2/s and a slip model with $k = 0{\cdot}2$, $0{\cdot}1$ cm/s

0·1 cm/s to 0·2 cm/s. This increased damping with decreasing thickness of the bottom boundary layer is to be expected, since for the vertical variation of eddy viscosity considered here (Distribution B in Figure 3) its depth mean value will increase as d_2 decreased, and hence the damping will increase.

To investigate how sensitive the damping of the free surface elevation is to changes in the functional form of the eddy viscosity in the bottom boundary layer, a series of calculations were performed using the eddy viscosity distribution (D) (Figure 3). Referring to this figure, $N_s = 2600\ \text{cm}^2/\text{s}$, $N_m = 650\ \text{cm}^2/\text{s}$, $N_h' = 100\ \text{cm}^2/\text{s}$ and N_h was varied, covering a range of values, namely $N_h = 1, 5, 10, 50\ \text{cm}^2/\text{s}$. The various thicknesses were $d_1 = 11$ m, $d_2 = 11$ m, $d_3' = 5{\cdot}5$ m. Thus, surface and mid-depth values of eddy viscosity were as in the previous calculations, and the thickness of surface and bottom layers remained unchanged. However the eddy viscosity in the bottom layer, no longer varied in essentially a linear manner, but had a value of $100\ \text{cm}^2/\text{s}$ at a height of 5·5 m above the sea bed.

The time variation of the sea surface elevation computed using this vertical variation of eddy viscosity is shown in Figure 7, for various values of N_h. Referring to this Figure, it is evident that as in the previous examples, the damping of the free surface elevation decreases as N_h decreases. Also for a given value of N_h, it can be readily seen comparing Figures 5–7, that the damping of ζ computed using the vertical eddy viscosity distribution D (Figure 3), is significantly less than that computed with distribution B (Figure 3). This is to be expected since the vertical mean viscosity in distribution D, is significantly less than that with distribution B, with corresponding values of N_s, N_m and N_h.

Current profiles, at position A, in the centre of the basin (Figure 1) at time $t = 90$ h (a time of near steady state) computed using a no-slip bottom boundary condition for the various eddy viscosity distributions B and D are shown in Figures 8–10. For comparision purposes, profiles calculated using a slip condition with the viscosity distribution C have also been plotted in these Figures.

Referring to Figures 8–10 it is apparent that for each eddy viscosity distribution, used in the no-slip model, as N_h increases the current near the sea bed decreases, due to the increased damping in this region. An interesting point is that the surface current shows a

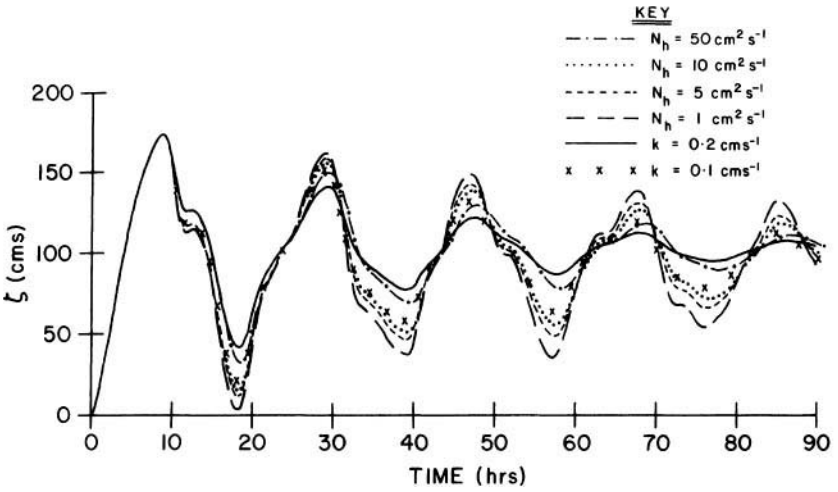

Figure 7. Time series of elevations ζ at corner point B, computed using a no slip model with $d_2 = 11$ m using eddy viscosity distribution (D) (see Figure 3), and $N_h = 50$, 10, 5, 1 cm^2/s and a slip model with $k = 0{\cdot}2$, 0·1 cm/s

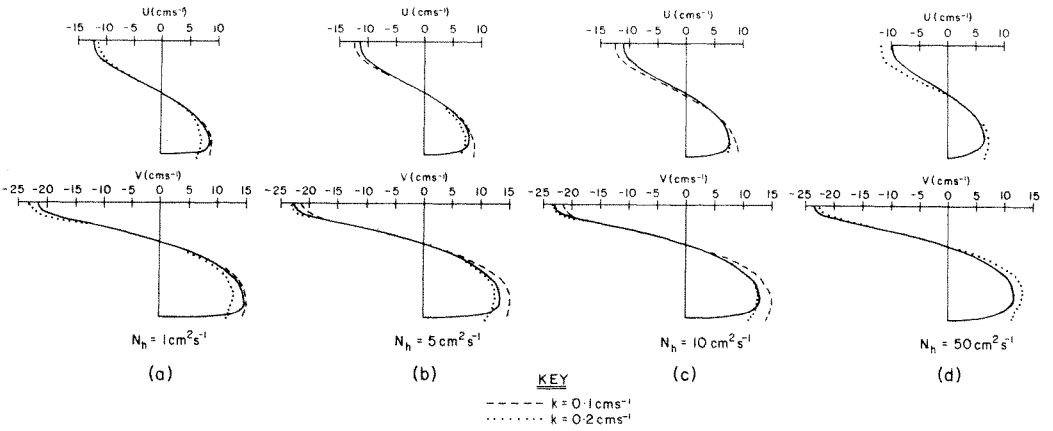

Figure 8. Current profiles at position A computed using viscosity distribution B (Figure 3) with $d_2 = 11$ m, $N_s = 2600$ cm^2/s, $N_m = 650$ cm^2/s and $N_h = 1, 5, 10, 50$ cm^2/s. For comparison purposes profiles computed with the slip model are also shown

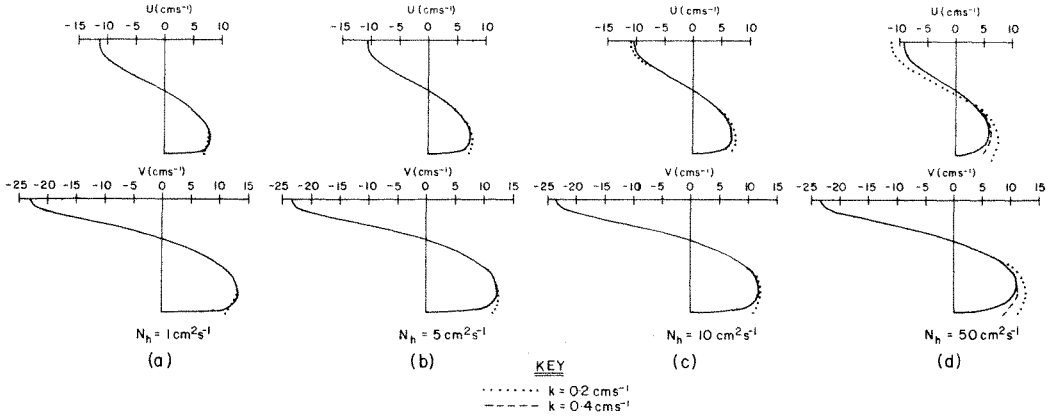

Figure 9. Current profiles at position A computed using viscosity distribution B (Figure 3) with $d_2 = 7$ m, $N_s = 2600$ cm^2/s, $N_m = 650$ cm^2/s and $N_h = 1, 5, 10, 50$ cm^2/s. For comparison purposes profiles computed with the slip model are also shown

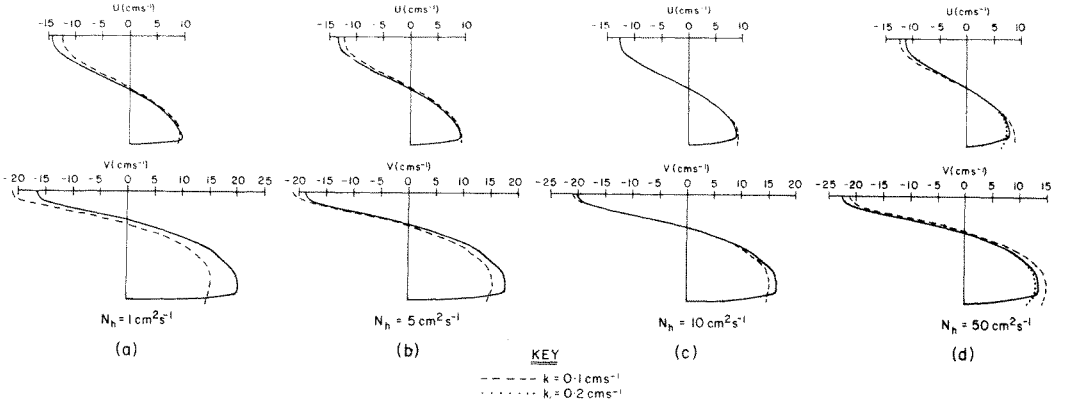

Figure 10. Current profiles at position A computed using viscosity distribution D (Figure 3) with $d_2 = 11$ m, $N_s = 2600$ cm^2/s, $N_m = 650$ cm^2/s and $N_h = 1, 5, 10, 50$ cm^2/s. For comparison purposes profiles computed with the slip model are also shown

slight but definite increase as N_h increases, however the reason for this is not clear. Decreasing the thickness of the bottom boundary layer with N_h fixed (compare Figures 8 and 9) slightly reduces currents near the sea bed. Changing the functional form of the eddy viscosity in such a manner that N is reduced in this region (Distribution D, Figure 3) produces a significant increase in bottom currents for a fixed N_h (compare Figures 8–10).

It is evident from these Figures that away from the sea bed, current profiles computed with a slip bottom boundary condition are not significantly different from those computed with some of the eddy viscosity distributions used here and a no-slip condition.

For example in Figure 8(a), the current profile computed with $N_h = 1$ cm^2/s, is comparable with that computed with $k = 0{\cdot}1$ cm/s. With $N_h = 10$ cm^2/s, the current profile resembles that computed with $k = 0{\cdot}2$ cm/s (Figure 8c). This correspondence between solutions computed using slip and no-slip bottom boundary conditions is also evident in the time variation of ζ (Figure 5). It is apparent from this figure that the curve computed with $N_h = 1$ cm^2/s is identical to that computed with $k = 0{\cdot}1$ cm/s and the solution with $N_h = 10$ cm^2/s corresponds to that computed with $k = 0{\cdot}2$ *cm/s.*

Current profiles computed with a bottom layer of thickness $d_2 = 7$ m are plotted in Figure 9. In this case, the profile computed with $N_h = 1$ cm^2/s matches that computed with $k = 0{\cdot}2$ cm/s. With a different functional form of viscosity near the sea bed, profiles computed with $N_h = 50$ cm^2/s, correspond to $k = 0{\cdot}2$ cm/s (Figure 10(d)).

These calculations clearly demonstrate that away from the close proximity of the sea bed, current profiles computed using a slip bottom boundary condition are not significantly different from those computed using a no-slip boundary condition.

In the case of a slip boundary condition with N_m and N_s constant there is only one free parameter k which determines the bottom stress. Increasing k produces more damping, whereas decreasing k reduces the damping. In the case of a no-slip bottom boundary condition again with N_m and N_s constant there are three factors which can produce a similar effect, namely the value of Z_0 and hence the magnitude of the viscosity at the sea bed, the thickness of the bottom boundary layer, and the functional form of the eddy viscosity in the bottom layer.

Bowden, Fairbairn and Hughes[20] have suggested that in tidal flow the vertical variation of eddy viscosity can be approximated by a linear increase of N with height above the sea bed, through a bottom layer of thickness $0{\cdot}14h$. Above this layer N is constant up to the sea surface. In the present model, $h = 65$ m, therefore $0{\cdot}14h = 9{\cdot}1$ m. Although flow in the model described here is wind induced, it does appear that a linear variation of viscosity in a bottom layer of the order of 9 m thick is consistent with current profiles and damping produced using a slip condition with a physically realistic value of k between $0{\cdot}1$ cm/s to $0{\cdot}2$ cm/s, (see Figure 8(a), 8(c) and 9(a)). Depending upon whether the bottom boundary layer is 7 m or 11 m thick, current profiles computed with this range of k values correspond to those computed with a range of N_h from 1 cm^2/s to 10 cm^2/s. Assuming a typical tidal current amplitude in the North Sea of 60 cm/s, using equation (45) (with $k_0 = 0{\cdot}41$, $K = 0{\cdot}005$), these values of N_h correspond to roughness lengths Z_0 of between $0{\cdot}57$ cm ($N_h = 1$ cm^2/s, current profiles comparable with $k = 0{\cdot}1$ cm/s) and $5{\cdot}7$ cm ($N_h = 10$ cm^2/s, current profiles comparable with $k = 0{\cdot}2$ cm/s). Both these roughness lengths appear acceptable and lie within the range of $7{\cdot}0$ cm to $0{\cdot}44$ cm observed by Channon and Hamilton.[17] The value of $Z_0 = 5{\cdot}7$ cm is consistent with the value of $k = 0{\cdot}2$ cm/s used in linear numerical models.[5,21]

However, recent observations[7] and theoretical work[8] have suggested that N may not vary in a linear manner but that its profile may show some curvature. Referring to Figure 10,

current profiles computed with viscosity distribution D which decreases rapidly near the sea bed (Figure 3), with $N_h = 50\ \text{cm}^2/\text{s}$ are not significantly different over the majority of the water column from those computed with $k = 0{\cdot}2$ cm/s. This value of N_h, implies that $Z_0 = 28{\cdot}0$ cm, a value higher than the range of values observed by Channon and Hamilton.[17]

Comparing Figures 8(c) and 10(d), it is evident that current profiles computed with a linear variation of viscosity near the sea bed (Figure 8(c)) are not significantly different from those computed with a non-linear variation (Figure 10(d)). However in order to obtain similar current profies different values of Z_0 have had to be used, namely $Z_0 = 5{\cdot}7$ cm (Figure 8(c)) and $Z_0 = 28{\cdot}0$ cm (Figure 10(d)).

This comparision illustrates the importance of knowing the exact variation of N in the bottom boundary layer, if the correct damping in the model is to be obtained without artificially having to increase Z_0. Having to increase Z_0 to 28·0 cm in order to obtain a physically realistic profile, suggest that N in this calculation, decreases too rapidly near the sea bed. However without more detailed information about how N should vary in the close proximity of the sea bed it is difficult to know precisely what variation should be used in a numerical model.

Comparisons of computed current profiles and damping of sea surface elevations, computed employing a model using a linear slip condition with $k = 0{\cdot}2$ cm/s and a model with a no-slip condition, suggests that the two models are consistent when the thickness of the bottom boundary layer is of the order of $0{\cdot}14h$ and Z_0 is of the order of 0·57 cm to 5·7 cm. This thickness of the bottom boundary layer and range of values of Z_0 are consistent with the vertical variation of N proposed by Bowden *et al.*[20] and values of Z_0 observed by Channon and Hamilton[17] and Heathershaw.[22]

The models used in these calculations are linear, however quadratic friction can be readily included using a slip condition at the sea bed,[11,16] and an eddy viscosity which is a function of position and time can also be included by using equation (44) to determine how α in equations (31) and (36) should vary with x, y and t.

5. CONCLUDING REMARKS

The numerical calculations presented in this paper show that the Galerkin method with a basis set of eigenfunctions (a Galerkin–eigenfunction method) has certain advantages over the application of the Galerkin method with a basis set of arbitrarily chosen functions.[2,4]

The principal restriction on the present method, as with all eigenfunction methods,[5,6] is that the functional form describing the vertical variation of eddy viscosity must be fixed. If this varies with time and horizontal space, then a new set of eigenfunctions must be computed at each time step and at each horizontal grid point in the model. Computationally this is not practical, and for the case in which the functional form of N in the vertical varies with time and space, the Galerkin method as formulated by Davies,[2,3] in which the form of N is completely general, is preferable.

However in many problems the vertical profile of eddy viscosity is fixed, although its magnitude varies with horizontal position and time.[8] In these circumstances the Galerkin–eigenfunction method as formulated in this paper can be applied with advantage.

Earlier eigenfunction methods[5,6] determined the eigenfunctions analytically and were therefore restricted to idealized, simple vertical variations of viscosity. In the present method the eigenfunctions are determined numerically, therefore the complex vertical variations of viscosity which are found in nature[7,8] can be included in the model.

The importance of using a high vertical resolution near the sea bed, with a no-slip bottom

boundary condition has been demonstrated in this paper. If a coarse vertical resolution is used, this has the physical effect of artificially increasing the value of N_h, the eddy viscosity at the sea bed. As has been demonstrated in Section 3, N_h is an important parameter which determines the damping of motion within the basin, and the magnitude of the free surface set-up in response to an applied wind stress.

Consistent values of sea surface elevation and currents computed using slip and no-slip models were obtain with, in the slip model, a value of $k = 0{\cdot}2$ cm/s a physically realistic value and a value of Z_0 between 0·57 cm and 5·7 cm, in the no-slip model. A bottom layer thickness of 7 m and 11 m was used in the no-slip model. These values of the bottom layer thickness agree with the value of $0{\cdot}14h = 9{\cdot}1$ m (in this case) determined from observations by Bowden, Fairbairn and Hughes.[20] The range of Z_0 values is in good agreement with observations made by Channon and Hamilton[17] and Heathershaw.[22]

The comparisons of current profiles computed using a slip and a no-slip model, with the above parameters, shows that away from the sea bed there are no significant differences in profiles computed with the two models. This confirms that currents away from the close proximity of the sea bed, computed using a slip bottom boundary condition, will not be significantly different from those computed with a no-slip boundary condition. By using a slip boundary condition, the problem of having to resolve the high shear layer near the sea bed does not occur. Also the difficulties of having to choose a value of Z_0, also a value for the thickness of the bottom layer and the functional form of viscosity to use in this layer, are avoided.

In practice values of Z_0 determined from observations can contain relatively large errors,[23] whereas values of C_{100} [the coefficient of friction to use in a three dimensional model[11]] are relatively accurate. In relation to the relative merits of Z_0 and C_{100}, Bowden[23] stated, 'On the whole the drag coefficient C_{100} appears to be a better parameter than Z_0 for relating the stress to the bottom roughness'. This statement appears to be as true in numerical modelling as in the physical world. The use of a slip bottom boundary condition, involving C_{100} in a numerical model, certainly appears to have advantages over the use of a no-slip boundary and the associated problem of deciding upon a value of Z_0, and how the viscosity should vary in the bottom boundary layer.

Although the model described here is linear, the extension of the Galerkin–eigenfunction method to a fully non-linear model can be readily accomplished in an analogous manner to that given by Davies.[3] In such a model, the value of the eddy viscosity would depend upon the magnitude of the currents hence it would vary with horizontal position and time. This variation would be incorporated in equations (31) and (36), by making α in these equations proportional to the currents.

Recently a model using a time and horizontally varying viscosity, with a slip bottom boundary condition, has been developed and successfully applied to the propagation of the M_2 tide from the Atlantic Ocean on to the North West European shelf.[16] The success of this model suggests that the use of an eddy viscosity which varies with horizontal position and time, but with a fixed vertical variation may be sufficient to accurately model the tides. Obviously, the Galerkin–eigenfunction method developed in this paper is ideal for the numerical solution of the hydrodynamic equations with this form of viscosity.

ACKNOWLEDGEMENTS

The author is indebted to Dr. N. S. Heaps for a number of suggestions in connection with this paper. The care and attention taken by Mrs L. Parry in typing this paper and Mr. R. A. Smith in preparing the diagrams is appreciated.

The work described in this paper was funded by a Consortium consisting of the Natural Environment Research Council, the Ministry of Agriculture, Fisheries and Food and the Department of Industry.

REFERENCES

1. B. Johns, 'The modelling of tidal flow in a channel using a turbulence energy closure scheme', *Journal of Physical Oceanography*, **8** (6) 1042–1049 (1978).
2. A. M. Davies, 'On formulating a three-dimensional hydrodynamic sea model with an arbitrary variation of vertical eddy viscosity', *Computer Methods in Applied Mechanics and Engineering*, **22,** 187–211 (1980).
3. A. M. Davies, 'Application of the Galerkin method to the formulation of a three-dimensional non-linear hydrodynamic numerical sea model', *Applied Mathematical Modelling*, **4,** 245–256 (1980).
4. A. M. Davies and A. Owen, 'Three-dimensional numerical sea model using the Galerkin method with a polynomial basis set', *Applied Mathematical Modelling*, **3,** 421–428 (1979).
5. N. S. Heaps, 'On the numerical solution of the three-dimensional hydrodynamical equations for tides and storm surges', *Mém. Soc. r. Sci. Liège Ser* 6, **2,** 143–180 (1972).
6. N. S. Heaps, 'Three-dimensional model for tides and surges with vertical eddy viscosity prescribed in two layers-I. Mathematical formulation', *Geophys. J.R. astr. Soc.*, **64,** 291–302 (1981).
7. J. Wolf, 'Estimation of shearing stresses in a tidal current with application to the Irish Sea Marine turbulence', (ed.) Nihoul, J. C. J. Elsevier Scientific Publishing Company, Amsterdam, 1980.
8. T. J. Smith, 'On the representation of Reynolds stress in estuaries and shallow coastal seas', submitted to *J.P.O.*
9. A. M. Davies, 'The numerical solution of the three-dimensional hydrodynamic equations using a B-spline representation of the vertical current profile', in Nihoul, J. C. J. (ed.) *Bottom Turbulence, Proceedings of the 8th Liege Colloquium on Ocean Hydrodynamics*, Elsevier, Elsevier Oceanography Series, **19,** 1977, pp. 1–25.
10. N. S. Heaps and J. E. Jones, 'Three-dimensional model for tides and surges with vertical eddy viscosity prescribed in two layers-II. Irish Sea with bed friction layer', *Geophys. J. R. astr. Soc.*, **64,** 303–320 (1981).
11. A. M. Davies and G. K. Furnes, 'Observed and computed M_2 tidal currents in the North Sea', *Journal of Physical Oceanography*, **10,** 237–257 (1980).
12. J. H. Wilkinson, *The Algebraic Eigenvalue Problem*, Oxford University Press, 1965.
13. J. H. Wilkinson, and C. Reinsch, *Handbook for Automatic Computation. Volume II, Linear Algebra*, Springer-Verlag, 1971, pp. 303–314, 212–226 and 227–240.
14. A. M. Davies, 'A numerical investigation of errors arising in applying the Galerkin method to the solution of non-linear partial differential equations', *Computer Meths. Appl. Mech. Eng.* **11,** 341–350 (1977).
15. W. H. Munk, and E. R. Anderson, 'Notes on a theory of the thermocline', *J. Marine Res.*, **1,** 276–295 (1948).
16. A. M. Davies, 'Three-dimensional hydrodynamic numerical models. Part 1. A homogeneous ocean-shelf model. Part 2. A stratified model of the Northern North Sea', *Proceedings of the Norwegian Coastal Current Symposium*, Geilo, Norway, 1981, published by Bergen University.
17. R. D. Channon, and D. Hamilton, 'Sea bottom velocity profiles on the Continental Shelf south-west of England', *Nature*, **231,** 383–385 (1971).
18. N. S. Heaps, 'Linearized vertically-integrated equations for residual circulaton in coastal seas', *Deutsche Hydrographische Zeitschrift*, **31,** 147–169 (1978).
19. K. F. Bowden, 'Note on wind drift in a channel in the presence of tidal currents', *Proc. Roy. Soc. London*, **A219,** 426–446 (1953).
20. K. F. Bowden, L. A. Fairbairn and P. Hughes, 'The distribution of shearing stresses in a tidal current, *Geophys, J. R. astr. Soc.* **2,** 288–305 (1959).
21. A. M. Davies and N. S. Heaps, 'Influence of the Norwegian Trench on the wind-driven circulation of the North Sea', *Tellus*, **32,** 164–175 (1980).
22. A. D. Heathershaw, 'The turbulent structure of the bottom boundary layer in a tidal current', *Geophys. J. R. astr. Soc.*, **58,** 395–430 (1979).
23. K. F. Bowden, 'Physical problems of the benthic boundary layer', *Geophysical Surveys*, **3,** 255–296 (1978).